ChemPubSoc Europe

DOI: 10.1002/cssc.201402171

Impact of the Electron-Transport Layer on the Performance of Solution-Processed Small-Molecule Organic Solar Cells

Guankui Long,[a] Xiangjian Wan,*[a] Bin Kan,[a] Zhicheng Hu,[b] Xuan Yang,[a] Yi Zhang,[a] Mingtao Zhang,[c] Hongbing Wu,[b] Fei Huang,[b] Shijian Su,[b] Yong Cao,[b] and Yongsheng Chen*[a]

Although the performance of polymer solar cells has been improved significantly recently through careful optimization with different interlayers for the same materials, more improvement is needed in this respect for small-molecule-based solar cells, particularly for the electron-transport layers (ETLs). In this work, three different solution-processed ETLs, PFN, ZnO nanoparticles, and LiF, were investigated and compared in the performance of small-molecule-based devices, and power conversion efficiencies (PCEs) of 8.32, 7.30, and 7.38% were achieved, respectively. The mechanism for the ETL-induced enhancement has been studied, and different ETLs have a significantly different impact on the device performance. The clearly improved performance of PFN is attributed to the combination of reduced bimolecular recombination and increased effective photon absorption in the active layer.

Introduction

Tremendous progress has been made in organic photovoltaics (OPVs) through the design and synthesis of low-bandgap donors, and power conversion efficiencies (PCEs) over 8% have been reached for both polymer and small-molecule-based solar cells.[1–4] However, device optimization, which includes the use of different interface layers, seems to play an important role to further optimize the short-circuit current density (J_{sc}) and fill factor (*FF*) for the same materials, by, for example, adjusting the work function of the charge-collecting electrodes, alternating the device absorptions or increasing the built-in potential across the device.[5–16] In general, LiF[17] and Ca[15] are the most widely used electron-transport layers (ETLs). However, the Ca/Al electrode is very unstable if exposed to air without encapsulation. The thickness and evaporation rate of LiF are also difficult to control (≈0.8–1 nm). For solution-processed ETLs, transition metal oxides (e.g., ZnO, TiO_x)[5,18] and some interesting polar organic ETLs[19] such as fullerene derivatives (neutral or surfactant),[6,20,21] nonconjugated polyelectrolytes (polyethylenimine derivatives such as PEIE, PEI; structures shown in Figure S1),[7,22] and conjugated polyelectrolytes such as polyfluorene derivatives, PFN, and PFCn6K (structures shown in Figure S1)[1,9,11,12,23,24] have been introduced into both conventional and inverted devices, and exciting performances have been achieved. So far, these ETLs have been used mainly in polymer-based organic photovoltaics (P-OPVs),[19,25] and few reports have focused on small molecules, especially solution-processed small-molecule-based organic photovoltaics (SM-OPVs).[3] Particularly, significantly higher performances have been achieved using PFN and ZnO NPs. If we consider the emergence of SM-OPVs[26–29] and their advantages, such as low batch-to-batch variation and easily controlled energy levels and absorption,[3,4,8,15,30–40] there is a demand to investigate the impact of various modifications, such as ETLs, on SM-OPVs systematically and to further optimize their device performance.

Our group has reported a series of A-D-A type oligothiophene derivatives that exhibited very promising performance for solution-processed OPV devices,[4,41–44] and PCEs of 7–8% have been achieved.[4] Among these molecules, 5,5′-({4,8-bis[(2-ethylhexyl)oxy]benzo[1,2-*b*:4,5-*b*′]dithiophene-2,6-diyl}bis{[3,3′′-dioctyl(2,2′:5′,2′′-terthiophene)-5′′,5-diyl]methylidyne})bis-(3-ethyl-2-thioxo-4-thiazolidinone) (DR3TBDT; Figure 1) has a centrosymmetric structure, zero ground state, and vertical excited-state dipole moments based on DFT calculations.[45] Furthermore, its transition dipole moment ($S_0 \rightarrow S_1$) is relatively large

[a] G. Long, Dr. X. Wan, B. Kan, X. Yang, Y. Zhang, Prof. Y. Chen
Key Laboratory of Functional Polymer Materials
Collaborative Innovation Center of Chemical Science and Engineering
Center for Nanoscale Science and Technology
Institute of Polymer Chemistry, College of Chemistry
Nankai University
Tianjin 300071 (PR China)
E-mail: xjwan@nankai.edu.cn
yschen99@nankai.edu.cn

[b] Z. Hu, Prof. H. Wu, Prof. F. Huang, Prof. S. Su, Prof. Y. Cao
Department Institute of Polymer Optoelectronic Materials and Devices
State Key Laboratory of Luminescent Materials and Devices
South China University of Technology
Guangzhou, 510640 (PR China)

[c] Dr. M. Zhang
College of Chemistry
Nankai University
Tianjin, 300071 (PR China)

Supporting Information for this article is available on the WWW under http://dx.doi.org/10.1002/cssc.201402171.

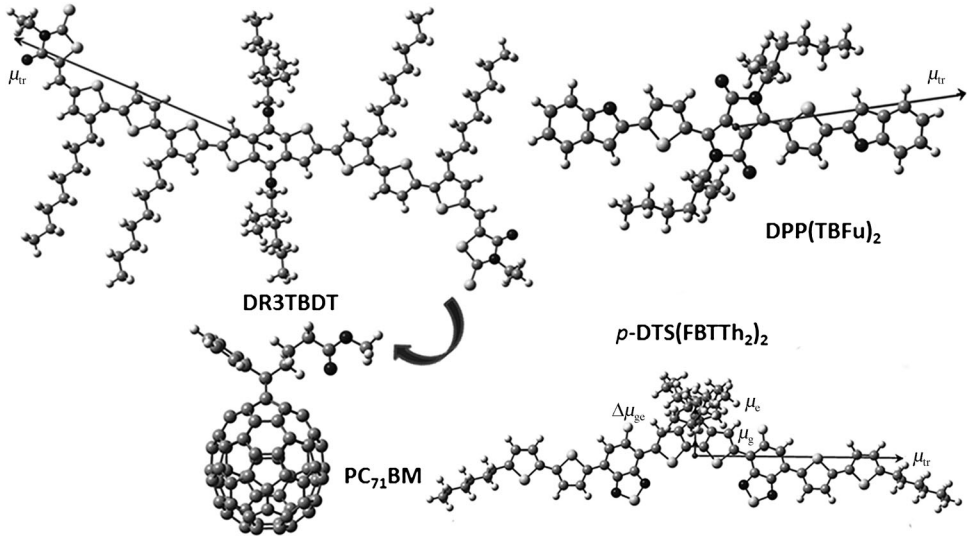

Figure 1. The optimized geometries for three representative small-molecule donors, DR3TBDT, DPP(TBFu)$_2$, and p-DTS(FBTTh$_2$)$_2$, and PC$_{71}$BM. The calculated ground and excited state and local and transition dipole moments ($S_0 \rightarrow S_1$) for these molecules are also shown for comparison.

(20.37 D) in the direction from the central benzodithiophene (BDT) core (donor unit) to the rhodanine end units, which is consistent with its strong absorption (Table S1).[35,46] Based on our calculations (Figure S2 and Table S2), its hole-reorganization energy (0.1994 eV) is also slightly lower than two other excellent small molecules (Figure 1), 3,6-bis[5-(benzofuran-2-yl)thiophen-2-yl]-2,5-bis(2-ethylhexyl)-pyrrolo-3,4-pyrrole-1,4-dione (DPP(TBFu)$_2$)[30] and 7,7′-[4,4-bis(2-ethylhexyl)-4*H*-silolo-3,2-b:4,5-b′-dithiophene-2,6-diyl]bis-[6-fluoro-4-(5′-hexyl-2,2′-bithiophen-5-yl)benzo-1,2,5-thiadiazole] (p-DTS(FBTTh$_2$)$_2$).[3] According to Marcus electron transfer theory, a small hole-reorganization energy implies less structural difference between the ground and cation state, which facilitates both charge transport in donor domains and charge transfer between the donor–acceptor interfaces.[47–49] These theoretical results and the exciting device performance with a PCE over 7% indicate that DR3TBDT is a promising donor and desirable for further device optimization. With this in mind, we wish to report the results and impact of two important ETLs, PFN and ZnO NPs, together with LiF as a comparison, on the performance of DR3TBDT-based devices. Through a systematic investigation, we have found that these ETLs have a significantly different impact on the device performance, and the PCE of 8.32% with PFN is attributed to the combination of reduced bimolecular recombination and increased effective photon absorption of the active layer.

Results and Discussion

Device performance with different ETLs

The optimized device performance parameters with different ETLs and the control device without ETL under the illumination of AM1.5G, 100 mW cm^{-2} are summarized in Table 1. Typical J–V curves of the optimized devices are shown in Figure 2. We also tested different thickness of ETLs on the device performance (Table S3). The control device without an ETL exhibited a moderate PCE of 5.47% with V_{oc} = 0.88 V, J_{sc} = 11.09 mA cm^{-2}, and FF = 0.56 (V_{oc} = open-circuit voltage; Table 1). If ZnO NPs were used as the ETL, an improved PCE of 7.30% with V_{oc} = 0.94 V, J_{sc} = 11.77 mA cm^{-2}, and FF = 0.66 was achieved. Similar results were obtained if LiF was used as the ETL. Notably, the device with PFN as an ETL exhibited a sharply enhanced PCE of 8.32% with an improved J_{sc} of 12.92 mA cm^{-2} and FF of 0.70. To the best of our knowledge, this PCE of 8.32% is among the highest efficiencies reported for small-molecule-[3,4] and polymer-based solar cells.[1] The series resistance (R_s) for the control device and the device with LiF, ZnO NPs, and PFN decreased from 8.35 to 8.02, 7.27, and

Table 1. Device performance parameters for bulk heterojunction (BHJ) solar cells based on DR3TBDT:PC$_{71}$BM (1:0.8 *w/w*, 0.2 mg mL^{-1} PDMS) with different ETLs.

ETL	V_{oc} [V]	J_{sc} [mA cm^{-2}]	FF	PCE [%]	PCE$_{ave}$ [%]	R_s [Ω cm^2]	R_{sh} [Ω cm^2]
None	0.88	11.09	0.56	5.47	5.36	8.35	411.23
LiF[a]	0.93	12.21	0.65	7.38	7.18	8.02	1221.37
ZnO	0.94	11.77	0.66	7.30	7.15	7.27	904.51
PFN	0.92	12.92	0.70	8.32	8.13	6.31	1905.49

[a] OPV data for LiF from Ref. [4a]

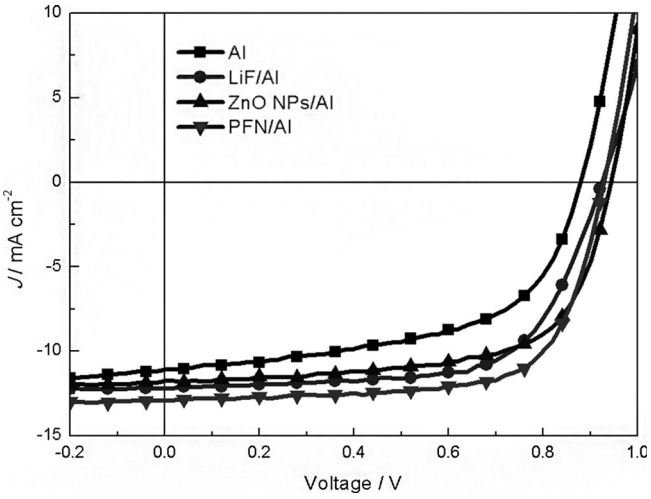

Figure 2. J–V curves of the devices ITO/PEDOT:PSS/DR3TBDT:PC$_{71}$BM (with PDMS)/with or without ETLs/Al under simulated 100 mW cm^{-2} AM1.5G illumination.

6.31 Ω cm^2, respectively (Table 1). Meanwhile, the shunt resistances (R_{sh}) increased significantly from 411.23 to 904.51, 1221.37, and 1905.49 Ω cm^2 for the control, ZnO NPs, LiF, and PFN devices, respectively. These trends are generally consistent with the improved FF for the devices.

The external quantum efficiency (EQE) spectra for the optimized devices based on DR3TBDT with and without ETLs are shown in Figure 3a. The EQE curve for the device with PFN exhibited a highly efficient photoelectron conversion efficiency

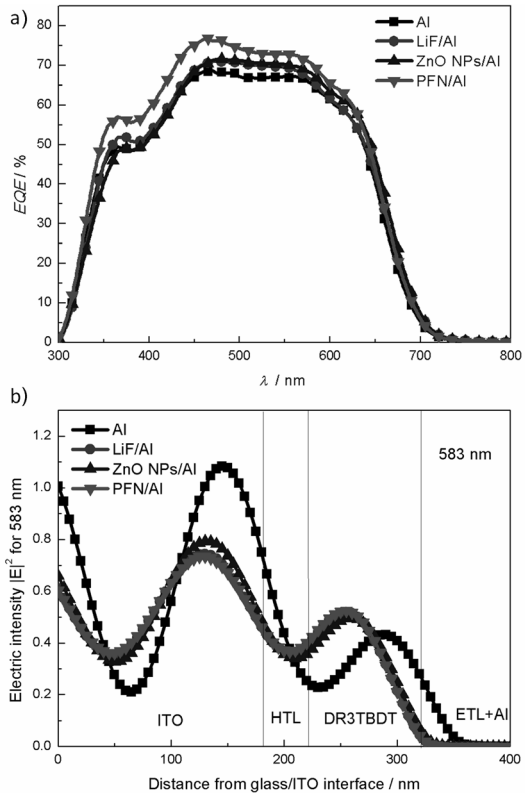

Figure 3. a) EQE spectra of the devices ITO/PEDOT:PSS/DR3TBDT:PC$_{71}$BM (with PDMS)/with or without ETLs/Al under simulated 100 mW cm^{-2} AM1.5G illumination. b) The simulated distribution of the squared optical electric field $|E|^2$ inside the devices with different ETLs at 583 nm.

from 320–650 nm than that of LiF, ZnO NPs, and the control devices, with the highest EQE value of 77% at 465 nm and an integrated J_{sc} of 12.19 mA cm^{-2}. In comparison, the device with LiF, ZnO NPs, and the control device showed a peak EQE of 71% at 470 nm,[4a] 72% at 480 nm, and 69% at 470 nm with integrated J_{sc} values of 11.50, 11.69, and 10.93 mA cm^{-2}, respectively. These results are consistent with the experimental and optical simulated results of the devices (Figure 3b and Figures S3 and S4) and prove that the incorporation of PFN as the ETL could indeed improve the J_{sc} and, therefore, the PCE.

The increased J_{sc} in the OPV devices may originate from reduced bimolecular recombination, the increased absorption of photons, or a combination of both.[1] The J_{sc} is an integration of EQE for the whole solar spectrum [Eq. (1)].[50] The EQE can be represented by the products of each efficiency in the following fundamental processes [Eq. (2)]:[51] light absorption (η_A), exciton diffusion (η_{ED}), exciton dissociation (η_{CD}), charge transport (η_{CT}), and charge collection at the electrodes (η_{CC}).[51,52]

$$J_{sc} = \frac{e}{hc}\int_{\lambda_1}^{\lambda_2} P_{AM1.5G}(\lambda)\cdot EQE(\lambda)\cdot \lambda d\lambda \quad (1)$$

$$\eta_{EQE} = \eta_A\eta_{IQE} = \eta_A\eta_{ED}\eta_{CD}\eta_{CT}\eta_{CC} \quad (2)$$

In the following section, we will discuss the effect of these ETLs on the above-mentioned fundamental processes in the OPV device from the optical simulations (η_A), photoluminescence (PL) spectra (η_{ED} and η_{CD}), hole mobility (η_{CT}), reverse-saturation dark current density ($J_{0,n}$), and diode ideality factors (η_{ED} and η_{CD}), reverse-saturation photocurrent density, and charge collection efficiency (η_{CC} and η_{CD}).

Optical simulations

To investigate the impact of different ETLs on the light intensity redistribution in the active layer, optical simulations were performed based on real device conditions by using a 1D transfer matrix model (TMM).[53–55] The refractive index (n) and extinction coefficient (k) of the active layer, LiF, ZnO NPs, and PFN were derived by using a spectroscopic ellipsometer (Figure S5). The optical electric field shifted to the middle of the active layer with the introduction of different ETLs, which could directly influence the J_{sc} (Figure 3b and Figure S2). The simulated J_{sc} (assuming IQE = 100%) for LiF-, ZnO NPs-, and PFN-based devices is 14.88, 12.62, and 14.70 mA cm^{-2}, respectively (Figure S4). Notably, if ZnO NPs are used, the devices give a relatively lower simulated J_{sc}. This might be attributed to the larger refractive index difference between ZnO NPs and the DR3TBDT:PC$_{71}$BM active layer than that with PFN and LiF (Figure S5).[56]

PL spectra and reverse-saturation dark current density

The efficiency of exciton diffusion and dissociation is typically gauged by comparing the PL quenching of the blend film to that of the neat material (Figure S6). The quenching efficiency of the blend film is 90.84% without considering the effect of different ETLs for DR3TBDT:PC$_{71}$BM (with PDMS) blend film, which indicates that the majority of excitons reach the interface without clear geminate recombination.

The dark injected current density J_{inj} versus the applied voltage for DR3TBDT:PC$_{71}$BM devices with different ETLs (Figure S7) was fitted exponentially using Equation (3)[57] to determine the reverse-saturation dark current density ($J_{0,n}$) and diode ideality factor (n_0).[57,58]

$$J_{inj} = J_{0,n}\exp\left(\frac{qV}{n_0 k_B T}\right) \quad (3)$$

In general, the magnitude of $J_{0,n}$ mainly indicates the rate of net charge recombination at the donor–acceptor interface.[59]

The $J_{0,n}$ for a LiF-, PFN-, or ZnO-NP-based device is five to seven orders of magnitude lower than that of the device without ETL with values of 4.44×10^{-9} mA cm^{-2} for LiF,[4b] 2.09×10^{-11} mA cm^{-2} for PFN, 1.35×10^{-10} mA cm^{-2} for ZnO NPs, and 1.41×10^{-4} mA cm^{-2} for the control device (Table S4). The diode ideality factor also decreased from 3.34 to 1.70, 1.52, and 1.36 for the devices without ETL, with LiF,[4b] ZnO NPs, and PFN, respectively, which indicates that the introduction of different ETLs would result in smaller recombination and enhanced *FF*.[16]

Based on the results above, it is clear that ETLs such as LiF, ZnO NPs, and particularly PFN could reduce the recombination significantly because of the smaller reverse-saturation dark current density and diode ideality factor, which, therefore, increases the exciton diffusion (η_{ED}) and exciton dissociation (η_{CD}) efficiency.[9] It was proved that the existence of an interface dipole moment produced by different ETLs (e.g., PFN, ZnO, LiF) could enhance the built-in potential across the device, which, therefore, improves the charge transport properties, eliminates the build-up of space charges, and reduces recombination losses, and has an effect on the exciton dissociation and charge collection efficiency.[8–9, 17]

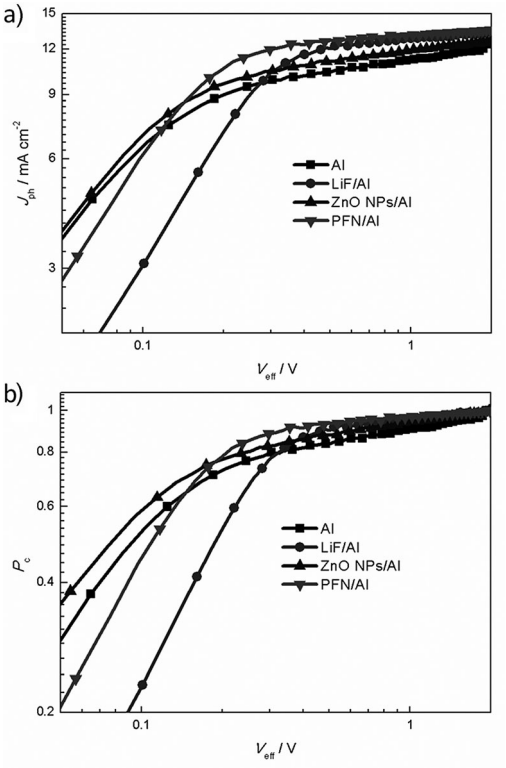

Figure 4. a) Net photocurrent density and b) charge collection efficiency versus effective voltage characteristics of devices with different ETLs and without the interlayer under constant incident light intensity (AM1.5G, 100 mW cm^{-2}).

Exciton generation, dissociation, and charge collection efficiency

The incorporation of the different interlayers could influence the exciton dissociation efficiency and charge collection efficiency under working conditions.[9, 13] The J_{ph}–V_{eff} characteristics in a wide reverse-bias range under AM1.5G illumination are shown in Figure 4a. The results are plotted as the net photocurrent density ($J_{ph}=J_L-J_D$) dependence on the effective applied voltage V_{eff} ($V_{eff}=V_0-V_{appl}$), in which J_L and J_D are the current density under illumination and in the dark, respectively, V_{appl} is the applied voltage, and V_0 is the compensation voltage at which $J_{ph}=0$.[9, 13, 60] Notably, J_{ph} reaches saturation for these devices at a larger reverse voltage (e.g., $V_{eff}=2$ V), which suggests that at this voltage nearly all the photogenerated excitons are dissociated into free carriers and all carriers are collected at the electrode without any bimolecular recombination. Under this circumstance, the photogenerated saturation current density ($J_{ph,sat}$) is then only limited by the total number of absorbed incident photons.[61] Here, J_L increases slightly at a large reverse bias (−2 V) because of the increase in J_D (higher leakage current density with higher reverse bias), but J_{ph} is almost constant over the applied negative voltage range (Figure S8). Therefore, our assumption that J_{ph} is saturated at an applied voltage of −1 V ($V_{eff}=2$ V) is confirmed.[15] With the assumption that all of the bound exciton pairs are dissociated in this case, the maximum generation rate of bound exciton pairs per unit volume (G_{max}) and the charge collection efficiency (P_c) of our OPV devices could be determined. G_{max} was calculated from Equation (4):

$$J_{ph,sat} = qG_{max}L \quad (4)$$

in which q is the electronic charge and L is the thickness of the active layer (≈100 nm). The values of G_{max} for the control device and devices with LiF, ZnO NPs, and PFN ETLs are 7.73×10^{27} ($J_{ph,sat}=12.38$ mA cm^{-2}), 8.16×10^{27} ($J_{ph,sat}=13.07$ mA cm^{-2}), 7.74×10^{27} ($J_{ph,sat}=12.40$ mA cm^{-2}), and 8.45×10^{27} m^{-3} s^{-1} ($J_{ph,sat}=13.54$ mA cm^{-2}), respectively. As G_{max} is related to the maximum absorption of incident photons, the increased G_{max} with ETLs suggests that there is better absorption in these devices (Figure 3b). An impressive increase in G_{max} was observed after the incorporation of the PFN or LiF layer, which is in agreement with the optical simulated $J_{sc,simu}$ results discussed above.

The exciton dissociation efficiency could also be obtained from the photocurrent density at the short-circuit condition ($J_{ph,sc}$) from Equation (5) and is 89.54, 94.55, and 96.59% for the control, LiF, and PFN devices (Figure 4b), which indicates that the incorporation of PFN should improve the exciton dissociation efficiency significantly. The exciton dissociation efficiency for the device with ZnO NPs is 93.22%, a little lower than that of the LiF-based device.

$$P_c = J_{ph,sc}/J_{ph,sat} \quad (5)$$

Interestingly, in the low effective voltage range ($V_{eff}<0.4$ V), the J_{ph}–V_{eff} characteristics for the devices with different ETLs are different. Under the maximal power output conditions ($V_{eff}=0.20$–0.23 V), $J_{ph,m}/J_{ph,sat}$ increased from 73.13% for the

control device to 79.49% for the device with LiF, 79.91% for that with ZnO NPs, and 81.95% for that with PFN. As $J_{ph,m}/J_{ph,sat}$ is the charge collection efficiency, a decreased $J_{ph,m}/J_{ph,sat}$ may indicate that bimolecular recombination begins to dominate, which usually leads to a lower *FF*.[9,15,61] The trend of $J_{ph,m}/J_{ph,sat}$ is consistent with the increase of *FF* from the control device to that with LiF, ZnO NPs, and PFN. The superior J_{ph}–V_{eff} characteristics of devices with different interlayers demonstrates clearly the effect that the interlayers could reduce bimolecular recombination at a low effective voltage and increase exciton generation and dissociation efficiency at a high effective voltage, which, therefore, improves the OPV performance.

Charge transport mobility

The ETLs have direct contact between the active layer and electrodes, which, therefore, would have a different impact on the extraction and collection of hole and electrons.[12] The effects of different ETLs on the charge transport properties for the optimized devices were investigated by using a hole-only device with the structure ITO/PEDOT:PSS/DR3TBDT:$PC_{71}BM$/ETL/Au (ITO = indium tin oxide, PEDOT:PSS = poly(3,4-ethylenedioxythiophene):poly(styrene sulfonate)) and an electron-only device with the structure Al/DR3TBDT:$PC_{71}BM$/ETL/Al.[62] The hole current density for PFN- and ZnO-NP-based devices increased by factors of 1.64 and 1.39, respectively, over that of the control device without an ETL (at 2×10^5 V cm^{-1}; Figure S9). The zero-field hole mobilities (μ_0; Table S5) for devices with LiF, ZnO NPs, and PFN are 1.12×10^{-3}, 8.27×10^{-4}, and 1.28×10^{-3} cm^{2}V^{-1}s^{-1}, respectively, which are higher than that of the control device (6.69×10^{-4} cm^{2}V^{-1}s^{-1}). The zero-field electron mobility for devices with LiF, ZnO NPs, and PFN is 5.31×10^{-4}, 2.04×10^{-3}, and 6.29×10^{-4} cm^{2}V^{-1}s^{-1}, respectively (Figure S10), and that of the control device is 8.54×10^{-5} cm^{2}V^{-1}s^{-1}. It is clear that the balance between hole and electron mobility is improved after the introduction of different ETLs. Among these ETLs, PFN gives the best balanced hole and electron mobility, which is consistent with the increased *FF* of 0.70, to give the best device performance.

Based on the discussion above for the optical simulations, exciton generation and dissociation, and charge transport and collection efficiency, it is clear that the improvement of each fundamental step in the photoelectron conversion process is expected if these ETLs are used, consistent with the experimental OPV results. Moreover, for the case of PFN, a combination of reduced bimolecular recombination and increased light absorption is believed to be the major reason for the significantly improved performance if it was used as the ETL.

Conclusions

The mechanism for the enhancement of solution-processed small-molecule-based organic photovoltaics induced by the electron-transport layer (ETL) has been investigated using different ETLs, and high power conversion efficiencies of 8.32 and 7.30% were achieved for devices based on PFN and ZnO nanoparticles, respectively. The performance improvements are attributed to the enhanced efficiencies of the exciton generation and dissociation, and charge transport and collection after the introduction of ETLs. If we consider the relatively scarce investigation of interlayers and other device-optimization techniques for small-molecule-based organic photovoltaics, it is highly likely that better performance could be obtained for the excellent small molecules reported recently if further device optimization is applied.

Experimental Section

Materials preparation

All reactions and manipulations were performed under an Ar atmosphere using standard Schlenk techniques. $PC_{71}BM$ was purchased from American Dye Source, Inc., and PDMS (trimethylsiloxy-terminated, MW = 14000) was purchased from Alfa Aesar. DR3TBDT was synthesized using our method reported previously.[4a] ZnO NPs were prepared using the technique described in Ref. [63], and PFN was obtained from SCUT.

Device fabrication and characterization

The photovoltaic devices were fabricated with the structure glass/ITO/PEDOT:PSS/DR3TBDT:$PC_{71}BM$/ETL/Al. The ITO-coated glass substrates were cleaned by ultrasonic treatment in detergent, deionized water, acetone, and isopropyl alcohol under ultrasonication for 15 min each and subsequently dried by blowing nitrogen. A thin layer of PEDOT:PSS (Baytron P VP AI 4083, filtered at 0.45 μm) was spin-coated (3000 rpm, ≈30 nm thick) onto an ITO surface. After they were baked at 150 °C for 20 min, the substrates were transferred to an Ar-filled glove box. Subsequently, the active layer was spin-cast from blend ratios (1:0.8 w/w) of DR3TBDT (8 mg mL^{-1}) and $PC_{71}BM$ with or without PDMS (0.2 mg mL^{-1}) in a chloroform solution at 1700 rpm for 20 s on the ITO/PEDOT:PSS substrate. PFN or ZnO NPs was spin-coated onto the active layer and LiF was vacuum deposited, and thermal annealing was performed at 75 °C for 10 min for the device based on ZnO NPs. Finally a 80 nm Al layer was deposited on the active layer under high vacuum ($<3\times10^{-4}$ Pa). The effective area of each cell was ≈4 mm^2 defined by masks. The thicknesses of the active layer and ZnO NPs were measured by using a Dektak 150 profilometer, and AFM was used to measure the thickness of the PFN.

The current density–voltage (*J*–*V*) curves of the photovoltaic devices were obtained by using a Keithley 2400 source-measure unit. The photocurrent was measured under illumination simulated at 100 mW cm^{-2} AM1.5G irradiation by using a xenon-lamp-based solar simulator (Oriel 96000 (AM1.5G)) in an Ar-filled glove box. The irradiance was calibrated by using a certified silicon diode.

EQE values of the encapsulated devices were measured by using a lock-in amplifier (SR810, Stanford Research Systems). The devices were illuminated by monochromatic light from a 150 W xenon lamp that passed through an optical chopper and a monochromator. Photon flux was determined by using a calibrated standard silicon photodiode.

Mobility measurements of DR3TBDT/$PC_{71}BM$ (1:0.8 w/*w*) blend films with 0.2 mg mL^{-1} PDMS were performed with the following diode structures: ITO/PEDOT:PSS/active layer/ETL/Au for hole and Al/active layer/ETL/Al for electron at the *J*–*V* curve in the range of 0–7 V. The charge carrier mobilities were calculated using the space-charge limited current (SCLC)[62] model [Eq. (6)]:

$$J = \frac{9\,\varepsilon_0\varepsilon_r\mu_0 V^2}{8\,L^3}\exp\left(0.89\,\beta\sqrt{\frac{V}{L}}\right) \quad (6)$$

in which J is the current density, L is the film thickness of the active layer, μ_0 is the zero-field hole mobility, ε_r is the relative dielectric constant of the transport medium, ε_0 is the permittivity of free space (8.85×10^{-12} F m^{-1}), β is the field activation factor, and V ($=V_{appl}-V_{bi}$) is the internal voltage in the device, in which V_{appl} is the applied voltage to the device and V_{bi} is the built-in voltage caused by the relative work function difference of the two electrodes.

Acknowledgements

The authors gratefully acknowledge the financial support from MoST (2012CB933401 and 2014CB643502), NSFC (21374050, 51273093 and 51373078), PCSIRT (IRT1257), and Tianjin city (13RCGFGX01121) and thank beamline BL14B1 (Shanghai Synchrotron Radiation Facility) for providing beam time.

Keywords: DFT calculations · electron transport · lithium fluoride · photochemistry · zinc oxide

[1] Z. He, C. Zhong, S. Su, M. Xu, H. Wu, Y. Cao, *Nat. Photonics* **2012**, *6*, 591 – 595.
[2] S. H. Liao, H. J. Jhuo, Y. S. Cheng, S. A. Chen, *Adv. Mater.* **2013**, *25*, 4766 – 4771.
[3] A. K. K. Kyaw, D. H. Wang, D. Wynands, J. Zhang, T. Q. Nguyen, G. C. Bazan, A. J. Heeger, *Nano Lett.* **2013**, *13*, 3796 – 3801.
[4] a) J. Zhou, X. Wan, Y. Liu, Y. Zuo, Z. Li, G. He, G. Long, W. Ni, C. Li, X. Su, Y. Chen, *J. Am. Chem. Soc.* **2012**, *134*, 16345 – 16351; b) J. Zhou, Y. Zuo, X. Wan, G. Long, Q. Zhang, W. Ni, Y. Liu, Z. Li, G. He, C. Li, B. Kan, M. Li, Y. Chen, *J. Am. Chem. Soc.* **2013**, *135*, 8484 – 8487.
[5] a) H. L. Yip, S. K. Hau, N. S. Baek, H. Ma, A. K.-Y. Jen, *Adv. Mater.* **2008**, *20*, 2376 – 2382; b) X. Gu, W. Cui, T. Song, C. Liu, X. Shi, S. Wang, B. Sun, *ChemSusChem* **2014**, *7*, 416 – 420.
[6] a) S. K. Hau, Y. J. Cheng, H. L. Yip, Y. Zhang, H. Ma, A. K.-Y. Jen, *ACS Appl. Mater. Interfaces* **2010**, *2*, 1892 – 1902; b) C. E. Song, K. Y. Ryu, S. J. Hong, C. Bathula, S. K. Lee, W. S. Shin, J. C. Lee, S. K. Choi, J. H. Kim, S. J. Moon, *ChemSusChem* **2013**, *6*, 1445 – 1454.
[7] Y. Zhou, C. Fuentes-Hernandez, J. Shim, J. Meyer, A. J. Giordano, H. Li, P. Winget, T. Papadopoulos, H. Cheun, J. Kim, M. Fenoll, A. Dindar, W. Haske, E. Najafabadi, T. M. Khan, H. Sojoudi, S. Barlow, S. Graham, J. L. Brédas, S. R. Marder, A. Kahn, B. Kippelen, *Science* **2012**, *336*, 327 – 332.
[8] A. K. K. Kyaw, D. H. Wang, V. Gupta, J. Zhang, S. Chand, G. C. Bazan, A. J. Heeger, *Adv. Mater.* **2013**, *25*, 2397 – 2402.
[9] Z. He, C. Zhong, X. Huang, W. Y. Wong, H. Wu, L. Chen, S. Su, Y. Cao, *Adv. Mater.* **2011**, *23*, 4636 – 4643.
[10] a) T. Yang, M. Wang, C. Duan, X. Hu, L. Huang, J. Peng, F. Huang, X. Gong, *Energy Environ. Sci.* **2012**, *5*, 8208 – 8214; b) A. Kumar, G. Pace, A. A. Bakulin, J. Fang, P. K. H. Ho, W. T. S. Huck, R. H. Friend, N. C. Greenham, *Energy Environ. Sci.* **2013**, *6*, 1589 – 1596; c) P. Cheng, Y. Li, X. Zhan, *Nanotechnology* **2013**, *24*, 484008.
[11] J. H. Seo, A. Gutacker, Y. Sun, H. Wu, F. Huang, Y. Cao, U. Scherf, A. J. Heeger, G. C. Bazan, *J. Am. Chem. Soc.* **2011**, *133*, 8416 – 8419.
[12] S. H. Liao, Y. L. Li, T. H. Jen, Y. S. Cheng, S. A. Chen, *J. Am. Chem. Soc.* **2012**, *134*, 14271 – 14274.
[13] L. Lu, Z. Luo, T. Xu, L. Yu, *Nano Lett.* **2013**, *13*, 59 – 64.
[14] W. Li, A. Furlan, K. H. Hendriks, M. M. Wienk, R. A. J. Janssen, *J. Am. Chem. Soc.* **2013**, *135*, 5529.
[15] A. K. K. Kyaw, D. H. Wang, V. Gupta, W. L. Leong, L. Ke, G. C. Bazan, A. J. Heeger, *ACS Nano* **2013**, *7*, 4569 – 4577.
[16] X. Guo, N. Zhou, S. J. Lou, J. Smith, D. B. Tice, J. W. Hennek, R. P. Ortiz, J. T. L. Navarrete, S. Li, J. Strzalka, L. X. Chen, R. P. H. Chang, A. Facchetti, T. J. Marks, *Nat. Photonics* **2013**, *7*, 825 – 833.
[17] C. J. Brabec, S. E. Shaheen, C. Winder, N. S. Sariciftci, P. Denk, *Appl. Phys. Lett.* **2002**, *80*, 1288 – 1290.
[18] J. Y. Kim, S. H. Kim, H. H. Lee, K. Lee, W. Ma, X. Gong, A. J. Heeger, *Adv. Mater.* **2006**, *18*, 572 – 576.
[19] C. Duan, K. Zhang, C. Zhong, F. Huang, Y. Cao, *Chem. Soc. Rev.* **2013**, *42*, 9071 – 9104.
[20] C. H. Hsieh, Y. J. Cheng, P. J. Li, C. H. Chen, M. Dubosc, R. M. Liang, C. S. Hsu, *J. Am. Chem. Soc.* **2010**, *132*, 4887 – 4893.
[21] K. M. O'Malley, C. Z. Li, H. L. Yip, A. K.-Y. Jen, *Adv. Energy Mater.* **2012**, *2*, 82 – 86.
[22] H. Kang, S. Hong, J. Lee, K. Lee, *Adv. Mater.* **2012**, *24*, 3005 – 3009.
[23] J. Kesters, T. Ghoos, H. Penxten, J. Drijkoningen, T. Vangerven, D. M. Lyons, B. Verreet, T. Aernouts, L. Lutsen, D. Vanderzande, J. Manca, W. Maes, *Adv. Energy Mater.* **2013**, *3*, 1180 – 1185.
[24] Y. M. Chang, R. Zhu, E. Richard, C. C. Chen, G. Li, Y. Yang, *Adv. Funct. Mater.* **2012**, *22*, 3284 – 3289.
[25] S. Chen, J. R. Manders, S. W. Tsang, F. So, *J. Mater. Chem.* **2012**, *22*, 24202 – 24212.
[26] B. Walker, C. Kim, T. Q. Nguyen, *Chem. Mater.* **2011**, *23*, 470 – 482.
[27] A. Mishra, P. Bäuerle, *Angew. Chem.* **2012**, *124*, 2060 – 2109; *Angew. Chem. Int. Ed.* **2012**, *51*, 2020 – 2067.
[28] Y. Lin, Y. Li, X. Zhan, *Chem. Soc. Rev.* **2012**, *41*, 4245 – 4272.
[29] Y. Chen, X. Wan, G. Long, *Acc. Chem. Res.* **2013**, *46*, 2645 – 2655.
[30] B. Walker, A. B. Tomayo, X. D. Dang, P. Zalar, J. H. Seo, A. Garcia, M. Tantiwiwat, T. Q. Nguyen, *Adv. Funct. Mater.* **2009**, *19*, 3063 – 3069.
[31] T. Rousseau, A. Cravino, E. Ripaud, P. Leriche, S. Rihn, A. De Nicola, R. Ziessel, J. Roncali, *Chem. Commun.* **2010**, *46*, 5082 – 5084.
[32] J. Shin, N. S. Kang, K. H. Kim, T. W. Lee, J. I. Jin, M. Kim, K. Lee, B. K. Ju, J. M. Hong, D. H. Choi, *Chem. Commun.* **2012**, *48*, 8490 – 8492.
[33] S. Loser, H. Miyauchi, J. W. Hennek, J. Smith, C. Huang, A. Facchetti, T. J. Marks, *Chem. Commun.* **2012**, *48*, 8511 – 8513.
[34] O. P. Lee, A. T. Yiu, P. M. Beaujuge, C. H. Woo, T. W. Holcombe, J. E. Millstone, J. D. Douglas, M. S. Chen, J. M. Fréchet, *Adv. Mater.* **2011**, *23*, 5359 – 5363.
[35] H. Bürckstümmer, E. V. Tulyakova, M. Deppisch, M. R. Lenze, N. M. Kronenberg, M. Gsäenger, M. Stolte, K. Meerholz, F. Würthner, *Angew. Chem.* **2011**, *123*, 11832 – 11836; *Angew. Chem. Int. Ed.* **2011**, *50*, 11628 – 11632.
[36] R. Fitzner, E. Mena-Osteritz, A. Mishra, G. Schulz, E. Reinold, M. Weil, C. Körner, H. Ziehlke, C. Elschner, K. Leo, M. Riede, M. Pfeiffer, C. Uhrich, P. Bäuerle, *J. Am. Chem. Soc.* **2012**, *134*, 11064 – 11067.
[37] J. Mei, K. R. Graham, R. Stalder, J. R. Reynolds, *Org. Lett.* **2010**, *12*, 660 – 663.
[38] G. Wei, S. Wang, K. Sun, M. E. Thompson, S. R. Forrest, *Adv. Energy Mater.* **2011**, *1*, 184 – 187.
[39] a) H. Shang, H. Fan, Y. Liu, W. Hu, Y. Li, X. Zhan, *Adv. Mater.* **2011**, *23*, 1554 – 1557; b) Y. Lin, L. Ma, Y. Li, Y. Liu, D. Zhu, X. Zhan, *Adv. Energy Mater.* **2014**, *4*, 201300626; c) Y. Lin, L. Ma, Y. Li, Y. Liu, D. Zhu, X. Zhan, *Adv. Energy Mater.* **2013**, *3*, 1166 – 1170.
[40] Y. Liu, Y. Yang, C. C. Chen, Q. Chen, L. Dou, Z. Hong, G. Li, Y. Yang, *Adv. Mater.* **2013**, *25*, 4657 – 4662.
[41] Y. Liu, X. Wan, F. Wang, J. Zhou, G. Long, J. Tian, J. You, Y. Yang, Y. Chen, *Adv. Energy Mater.* **2011**, *1*, 771 – 775.
[42] J. Zhou, X. Wan, Y. Liu, G. Long, F. Wang, Z. Li, Y. Zuo, C. Li, Y. Chen, *Chem. Mater.* **2011**, *23*, 4666 – 4668.
[43] Z. Li, G. He, X. Wan, Y. Liu, J. Zhou, G. Long, Y. Zuo, M. Zhang, Y. Chen, *Adv. Energy Mater.* **2012**, *2*, 74 – 77.
[44] Y. Liu, X. Wan, F. Wang, J. Zhou, G. Long, J. Tian, Y. Chen, *Adv. Mater.* **2011**, *23*, 5387 – 5391.
[45] Gaussian 09, Revision B.01, Gaussian, Inc., Wallingford CT, **2010**, see the Supporting Information for full citation.
[46] B. Carsten, J. M. Szarko, H. J. Son, W. Wang, L. Lu, F. He, B. S. Rolczynski, S. Lou, L. Chen, L. Yu, *J. Am. Chem. Soc.* **2011**, *133*, 20468 – 20475.
[47] R. A. Marcus, *Rev. Mod. Phys.* **1993**, *65*, 599 – 610.
[48] J. L. Brédas, D. Beljonne, V. Coropceanu, J. Cornil, *Chem. Rev.* **2004**, *104*, 4971 – 5003.
[49] L. Wang, G. Nan, X. Yang, Q. Peng, Q. Li, Z. Shuai, *Chem. Soc. Rev.* **2010**, *39*, 423 – 434.

[50] G. Dennler, M. C. Scharber, C. J. Brabec, *Adv. Mater.* **2009**, *21*, 1323 – 1338.
[51] J. Guo, H. Ohkita, H. Benten, S. Ito, *J. Am. Chem. Soc.* **2010**, *132*, 6154 – 6164.
[52] N. S. Sariciftci, L. Smilowitz, A. J. Heeger, F. Wudl, *Science* **1992**, *258*, 1474 – 1476.
[53] P. Peumans, A. Yakimov, S. R. Forrest, *J. Appl. Phys.* **2003**, *93*, 3693 – 3723.
[54] G. F. Burkhard, E. T. Hoke, M. D. McGehee, *Adv. Mater.* **2010**, *22*, 3293 – 3297.
[55] L. A. A. Pettersson, L. S. Roman, O. Inganäs, *J. Appl. Phys.* **1999**, *86*, 487 – 496.
[56] Z. Tan, L. Li, F. Wang, Q. Xu, S. Li, G. Sun, X. Tu, X. Hou, J. Hou, Y. Li, *Adv. Energy Mater.* **2014**, *4*, 1300884.
[57] K. Vandewal, K. Tvingstedt, A. Gadisa, O. Inganäs, J. V. Manca, *Nat. Mater.* **2009**, *8*, 904 – 909.
[58] G. Long, X. Wan, B. Kan, Y. Liu, G. He, Z. Li, Y. Zhang, W. Y. Zhang, Q. Zhang, M. Zhang, Y. Chen, *Adv. Energy Mater.* **2013**, *3*, 639 – 646.
[59] C. Schlenker, M. Thompson, *Top. Curr. Chem.* **2012**, *312*, 175 – 212.
[60] P. W. Blom, V. D. Mihailetchi, L. J. Koster, D. E. Markov, *Adv. Mater.* **2007**, *19*, 1551 – 1566.
[61] S. R. Cowan, N. Banerji, W. L. Leong, A. J. Heeger, *Adv. Funct. Mater.* **2012**, *22*, 1116 – 1128.
[62] G. G. Malliaras, J. R. Salem, P. J. Brock, C. Scott, *Phys. Rev. B* **1998**, *58*, R13411 – R13414.
[63] W. J. E. Beek, M. M. Wienk, M. Kemerink, X. Yang, R. A. J. Janssen, *J. Phys. Chem. B* **2005**, *109*, 9505 – 9516.

Received: March 13, 2014
Revised: March 23, 2014
Published online on July 1, 2014